Journal of Materials Chemistry A

Accepted Manuscript

ROYAL SOCIETY OF CHEMISTRY

www.rsc.org/materialsA

Journal of Materials Chemistry A

Journal of Materials Chemistry A

Dynamic Article Links ►

Cite this: DOI: 10.1039/c0xx00000x

PAPER

www.rsc.org/xxxxxx

Ultraviolet photocatalytic degradation of methyl orange by nanostructured TiO_2/ZnO heterojunctions

Ruhua Zha,[a] Reddeppa Nadimicherla,[a] Xin Guo*[a]

Received (in XXX, XXX) Xth XXXXXXXXX 20XX, Accepted Xth XXXXXXXXX 20XX

DOI: 10.1039/b000000x

Nanostructured TiO_2/ZnO heterojunctions with the morphologies of hedgehogs and fan blades were synthesized by a solvothermal method, and characterized by means of XRD, SEM, TEM, BET, FT-IR, Raman, XPS, UV–vis and PL diffuse reflection spectroscopy. The photocatalytic activities of both TiO_2/ZnO hedgehogs and fan blades for the degradation of methyl orange (MO) were explored under UV light; the hedgehogs exhibited the best photocatalytic activity (97% MO degradation within 30 min) owing to the hierarchical nanostructure with large surface area. And the degradation mechanism was discussed based on the band structure. Both heterojunctions are very promising for the degradation of MO from organic dyestuff in engineering practices.

Introduction

Organic pollution from the anthropogenic wastewater is a common environmental concern,[1] therefore, many technologies have been developed to treat organic pollutants. The photocatalytic degradation technique based on semiconductors is highly effective, inexpensive and environmentally friendly.[2-4] During past decades, a variety of semiconductor photocatalysts, e.g. metal oxides,[5,6] nitrides[7-9] and sulfides,[10,11] have been investigated under UV light irradiation aiming at improving photocatalytic activities. However, the photocorrosion and short lifetime of photogenerated electron-hole pairs limited the UV-light responses and hindered their extensive applications.[12] In order to solve these problems, the recent research works focused on the preparation of special materials with various heterostructures[13-15] and high surface areas.[16-18] Yu and co-workers reported novel Ag_2O/Ag_2CO_3 heterostructured photocatalysts via phase transformation route,[19] the as-obtained heterostructures exhibit extremely high activity and stability for methyl orange and phenol decomposition under visible light irradiation. Similar result was found in MoS_2/CdS[20] and TiO_2/Ag_2CO_3[21] systems. Semiconductor heterostructures are necessary to promote the separation of photogenerated charge carries and to increase the lifetime.[22,23] Li et al.[24] suggested that the surface-phase junction of a semiconductor catalyst directly contributes to the photocatalytic reaction, therefore, tailoring the phase interface/junctions between the semiconductors could be effective in improving the photocatalytic activity. However, the controllable synthesis of different semiconductor heterostructures with high photocatalytic activity still remains a challenge.

Titanium dioxide (TiO_2) and zinc oxide (ZnO) are two technologically important semiconductors because of their applications in advanced systems and devices.[25–27] When exposed to an appropriate light source, TiO_2 and ZnO can generate photoinduced electron/hole (e^-/h^+) pairs to initiate a series of chemical reactions and eventually decompose the pollutants.[28] However, they can absorb only a small portion of the solar spectrum in the ultraviolet (UV) region because of their wide band gap energies (3.37 eV for ZnO, 3.2 eV for TiO_2) and high recombination rates of photoinduced e^-/h^+ pairs at or near their surfaces. Besides, the photocatalytic performance of ZnO nanocrystals is strongly dependent on their crystal nanostructures and morphologies at the nanometer scale.[29] Yu et al.[30] reported that the unique hollow Pt-ZnO nanocomposites with hierarchical structure showed enhanced photocatalytic activity and stability in decomposition of dye. Hence, to make TiO_2 and ZnO suitable for receiving and utilizing solar energy with high efficiency, many methods such as dye sensitization[31,32] and doping TiO_2 or ZnO[33–36] have been investigated. By a sonochemical method, Xue et al.[37] obtained hierarchical TiO_2/CdS hollow heterostructures with excellent visible light activity. Because the photocatalytic process is based on the generation of e^-/h^+ pairs by means of band gap radiation, the coupling of different semiconductor oxides seems very promising for achieving a more efficient e^-/h^+ pair separation under irradiation, and consequently, a higher photocatalytic activity. Currently, research interests have centered around design and synthesis of TiO_2/ZnO composite nanoparticles,[38,39] nanofilms[40,41] and many other hybrid nanostructured materials,[42,43] among which the coupled photocatalysts consisting of TiO_2 and ZnO exhibit significantly enhanced photocatalytic activities resulting from the synergic

effect.

The coupling of two semiconductors possessing different redox energy levels for the conduction bands (CB) and valence bands (VB) provides an attractive approach to achieve more efficient charge separation, increase the lifetime of charge carriers, and enhance the efficiency of interfacial charge transfer. The energy level for electron injection can be decreased when ZnO nanostructure covers the surface of TiO_2, which reduces the level of recombination between electrons and holes. And ZnO can increase the concentration of free electrons in the CB of TiO_2, therefore, the charge recombination can also be reduced in the process of electron transport.

In this work, we successfully synthesized TiO_2/ZnO heterojunctions with unusual morphologies, namely hedgehogs and fan blades. Both TiO_2/ZnO heterojunctions possessed favorable recycling characteristics, and exhibited enhanced photocatalytic activity in the decomposition of methyl orange (MO) under UV-light irradiation. MO is a typical pollutant in the textile industry[44] and was used as a model compound in this work. The degradation kinetics was pretty fast, which could be completed within 30 minutes. More importantly, the degradation capacity of both the TiO_2/ZnO heterojunctions did not show any obvious decrease after five degradation cycles. It is envisioned that our work might provide new insights for the semiconductor hybrid nanostructures.

2. Experimental

2.1. Preparation of TiO_2/ZnO heterojunctions

2.1.1. Hedgehogs

In a typical hedgehogs synthesis procedure, 0.17 g of TiF_4 (Alfa Aesar, 98%), 1 g NaF and 0.45 g $CO(NH_2)_2$ (Alfa Aesar, AR) were poured into 40 mL absolute ethanol (Alfa Aesar, AR) solution during vigorous stirring for 60 minutes to form a mixed solution (bottle A). And 0.6 g of $Zn(Ac)_2.2H_2O$ (Alfa Aesar, AR) and 0.3 g $C_6H_{12}N_4$ (Alfa Aesar, AR) were added to 45 mL distilled water solution during strong stirring for 60 minutes (bottle B). Then bottle B was added into bottle A and stirred again for another 60 minutes, the resulting solution was then transferred into a 100 mL Teflon-lined stainless steel autoclave and treated solvothermally at 160 °C for 24 h, and afterwards cooled down to room temperature. The final products were centrifuged, and rinsed with distilled water and ethanol several times and finally dried in oven at 60 °C overnight.

2.1.2. Fan blades

In a typical fan blades synthesis procedure, 0.17 g of TiF_4 (Alfa Aesar, 98%) and 0.55 g $CO(NH_2)_2$ (Alfa Aesar, AR) were poured into 40 mL absolute ethanol (Alfa Aesar, AR) solution during vigorous stirring for 60 minutes to form a mixed solution (bottle A). And 0.8 g of $Zn(Ac)_2.2H_2O$ (Alfa Aesar, AR), 0.01 g trisodium citrate (Alfa Aesar, AR) and 0.5 g $C_6H_{12}N_4$ (Alfa Aesar, AR) were added into 45 ml distilled water during strong stirring for 60 minutes (bottle B). Then bottle B was added into bottle A and stirred again for another 60 minutes, the resulting solution was then transferred into a 100 mL Teflon-lined stainless steel autoclave and treated solvothermally at 160 °C for 24 h, and afterwards cooled down to room temperature. Further procedures were the same as those of hedgehogs.

2.2. Characterization of TiO_2/ZnO heterostructures

Powder X-ray diffraction (XRD) patterns were measured by means of a Philips diffractometer (PW 3050) operated at 40 kV and 40 mA with Cu-Kα monochromatic radiation, at the Bragg's angle range from 20 to 80°. The heterojunctions of TiO_2/ZnO were observed by scanning electron microscope (SEM, Nova NanoSEM450). Transmission electron microscopy (TEM) investigations were carried out using a JEOL 2100F microscope. Nitrogen adsorption and desorption isotherms were determined by nitrogen physisorption at -196 °C with a Micrometritics ASAP 2020 analyzer. The pore size distribution (PSD) was calculated via a non-local density functional theory (NLDFT) method by using nitrogen adsorption data and assuming a slit pore model.[45,46] The chemical characteristics of adsorbents were analyzed by a Bruker VERTEX 70 Fourier transform infrared spectrometer (FT-IR). X-ray photoelectron spectroscopy (XPS) measurements were performed on a VG MultiLab 2000 system with a monochromatic Al Ka X-ray source (ThermoVG Scientific). The binding energy values were calibrated with the C 1s signal at 284.5 eV. The photoluminescence (PL) spectra of photocatalysts were detected with a Jobin Yvon HR800 micro-Raman spectrometer using a 325 nm line from a He-Cd laser. Raman spectra of the samples were collected at room temperature by a micro-Raman spectroscope (HR-800 LabRaman, Jobin Yvon, Longjumeau, France). The system included an integral Raman microscope, a stigmatic single spectrograph and a Peltier-cooled charge coupled device detector. The microscope attachment was an Olympus BX41 system using excitation with 10 mW Ar^+ laser light (k = 514.532 nm). The spectral resolution was about 1–2 cm^{-1}. UV-vis diffuse reflectance spectra were recorded on a SHIMADZU UV-2550 spectrophotometer with an integrating sphere, and $BaSO_4$ was used as a reference.

2.3. Evaluation of Photocatalytic Activity

The photocatalytic reaction was carried out in a photochemical reactor, which was a self-made cylindrical glass vessel with a water-cooling jacket. The photocatalytic activity of samples was characterized by the degradation of MO under UV light irradiation to a 500 W Hg lamp at ambient temperature. The irradiation distance between lamp and sample was 12 cm. In a typical procedure, 0.1 g of prepared photocatalyst was added into 100 mL of MO solution. The concentration of the MO solution was 20 mg mL^{-1}. The suspension was stirred for 30 min in dark place to reach an adsorption-desorption equilibrium of MO molecules on the surface of photocatalysts and then exposed to a 500 W Hg arc lamp. At a given time interval, 3 mL of reaction solution was taken out from suspension and immediately centrifuged at 18000 rev per min for 3 min. The top solution was exposed to absorption spectrum by UV/Vis spectroscopy (Shimadzu UV2550) in the range of 300–600 nm. The reaction was performed under constant magnetic stirring under ambient condition.

3. Results and Discussion

Journal of Materials Chemistry A

Journal of Materials Chemistry A

Dynamic Article Links ►

Cite this: DOI: 10.1039/c0xx00000x

PAPER

www.rsc.org/xxxxxx

3.1. Characterization of hedgehogs and fan blades

XRD analysis was employed to investigate the crystal phase of TiO_2 and TiO_2/ZnO heterojunctions (Fig. 1); the crystal phase of TiO_2 was anatase phase, and all the diffraction peaks of the TiO_2/ZnO heterojunctions could be indexed as hexagonal wurtzite-type (space group: P63mc) ZnO and the anatase TiO_2.

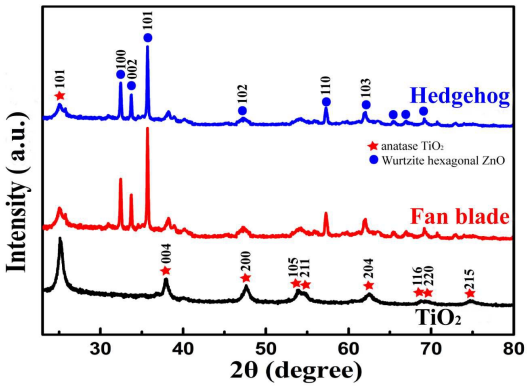

Fig. 1 XRD patterns of TiO_2 and TiO_2/ZnO hedgehogs and fan blades.

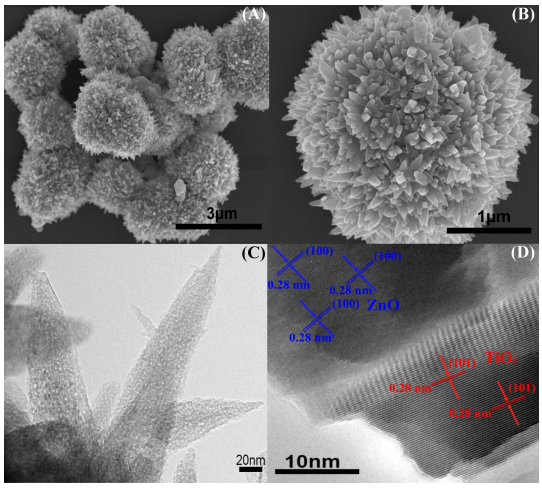

Fig. 2 (A and B) SEM images, (C) TEM image and (D) HRTEM image of hedgehogs.

The SEM and TEM images of hedgehogs are shown in Fig. 2. As shown in Figs. 2A–C, the hedgehogs were ~3 μm in diameter, and consisted of numerous mesoporous nanorods with a typical diameter of 60 nm and a length of 300–350 nm. To clearly reveal the nanostructure of hedgehogs, high-resolution transmission electron microscopy (HRTEM) observations were carried out, and the typical image result is shown in Fig. 2D. The simultaneous presence of crystal lattices of crystallized ZnO and TiO_2 in hedgehogs is clearly visible. The lattice fringes in the lower part could be assigned to the *d* spacing value of (101) planes in the anatase TiO_2. While the interplanar distances of 0.280 nm in the upper part agreed well with the lattice spacing of the (100) planes in the hexagonal wurtzite ZnO.

Fig. 3 depicts the plausible formation mechanism of hedgehogs via a three-step process.[47] Firstly, TiO_2 and ZnO nanoparticles were quickly formed in the solution and spontaneously aggregated to form large microspheres to minimize the surface area. Afterwards, the crystal growth process was transferred to a kinetically controlled process. The crystal growth was initiated preferentially from the active nanoparticles on the surfaces of microspheres. In the presence of F^- ions as a morphology controlling agent, these clusters were served as seeds for the subsequent growth along the *c* axis throughout the whole growth stage, by which the hedgehogs were formed.

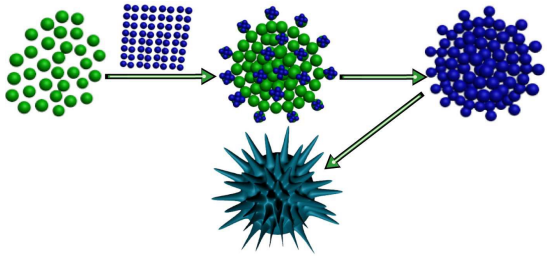

Fig. 3 Schematic illustration of the formation process of hedgehog.

The SEM and TEM images of fan blades are shown in Fig. 4, the fan blades consisted of multi-layers with a length of 2.5-3 μm. The HRTEM image is shown in Fig. 4D, the lattice fringes in the lower part could be assigned to the *d* spacing value of (101) planes in the anatase TiO_2, and the interplanar distances of 0.280 nm in the upper part agreed well with the lattice spacing of the (100) planes in the hexagonal wurtzite ZnO.

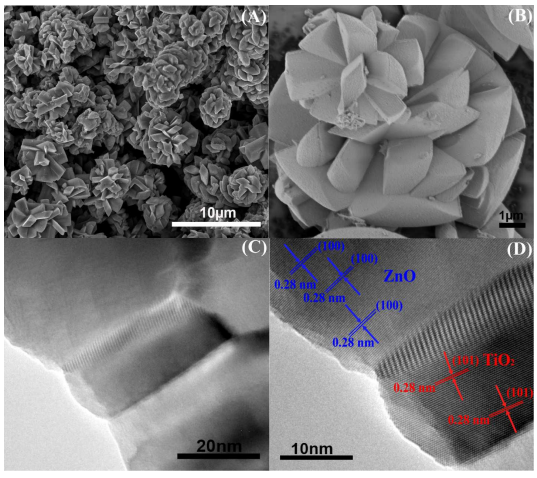

Fig. 4 (A and B) SEM images, (C) TEM image and (D) HRTEM image of fan blades.

Fig. 5 shows the possible formation process of the fan blades. The fan blades were also plausibly formed in three steps. At the beginning of reaction, TiO_2 and ZnO nanoparticles were produced in the solution then these nanoparticles were quickly aggregated into nanobulks. Afterwards these nanobulks spontaneously generated a dissolution-recrystallization process by the Ostwald ripening.[48] As the reaction time continued, trisodium citrate as a structure-modifying agent[49,50] exerted significant influence on the nucleation and growth process of TiO_2/ZnO crystals. As a result, the fan blades were generated.

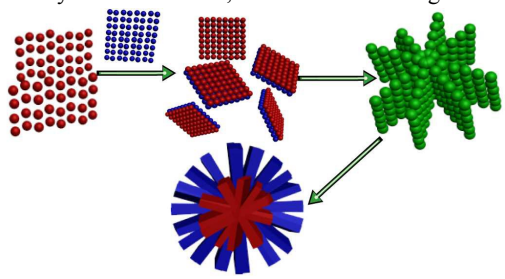

Fig. 5 Schematic illustration of the formation process of fan blade.

The BET curves of the hedgehogs and fan blades are depicted in Fig. 6, which describe nitrogen adsorption–desorption isotherms and their corresponding pore size distributions. Both hedgehogs and fan blades showed type II isotherms, which was a normal form of isotherm obtained with a mesopore adsorbent. The BET surface areas of hedgehogs and fan blades were found to be 96 and 56 $m^2\ g^{-1}$, respectively, and their average pore sizes were 4.0 and 4.3 nm, respectively. The type II isotherm represents unrestricted monolayer-multilayer adsorption.[51] The narrow pore size distribution for hedgehogs was consistent with their uniform morphologies.

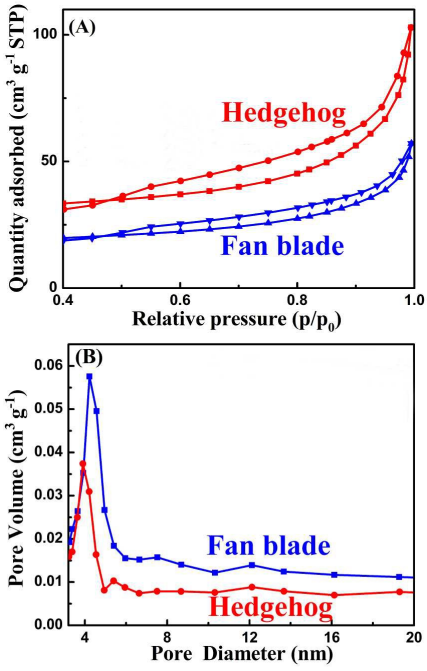

Fig. 6 (A) Nitrogen adsorption-desorption isotherms and (B) corresponding pore size distributions of TiO_2/ZnO hedgehogs and fan blades.

Fig. 7 illustrates the FT-IR spectra of TiO_2/ZnO heterojunctions and TiO_2. The broad peaks observed at 3434.8 cm^{-1} correspond to the stretching vibration of surface hydroxyls and adsorbed water,[52] the peaks at 1635.9 cm^{-1} are due to the bending vibration of Ti–OH,[53] the bands at about 1409.9 cm^{-1} are related to the bending vibration of Ti–O–Ti, and the peaks at 1118.7 cm^{-1} can be attributed to the Ti−O asymmetric vibration for TiO_2.[54,55] These characteristic peaks were blue-shifted to 3424.8, 1624.8, 1401.8 and 1019.6 cm^{-1}, respectively, in TiO_2/ZnO heterojunctions. Particularly, the intensity of the Ti−O peak (1118.7 cm^{-1}) in TiO_2 was greatly reduced (circle A) in the heterojunctions, accompanying with substantial wavenumber shift of 99.1 cm^{-1} (1118.7 to 1019.6 cm^{-1}), which evinced that the Ti−O bonds of TiO_2 were partly replaced by the Zn−O bonds in the heterojunctions, and Zn−O−Ti linkage was generated at the interfaces between ZnO and TiO_2. In addition, the pronounced peak at 490.6 cm^{-1} corresponds to the Zn−O bond (circle B).[56,57]

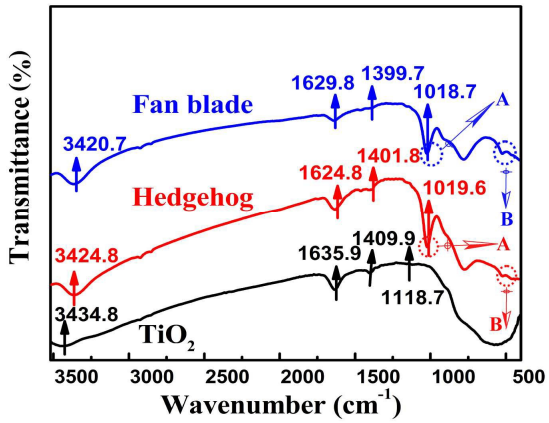

Fig. 7 FT-IR spectra of TiO_2 and TiO_2/ZnO hedgehogs and fan blades.

The Raman spectra of hedgehogs and fan blades are given in Fig. 8. The strong bands at 144.9, 396.9, 515.9 and 638.7 cm^{-1} corresponded to the anatase phase. All these characteristic bands were due to four Raman-active modes of anatase phase with the symmetries of E_g, B_{1g}, B_{1g} and E_g,[58] respectively. However, these characteristic peaks of TiO_2 were blue-shifted to 144.3, 396.4, 515.5 and 638.4 cm^{-1}, respectively, in the TiO_2/ZnO heterojunctions. The E_g peak of the hedgehogs was stronger than that of the fan blades, demonstrating that the content of oxygen vacancy in the hedgehogs was larger than that in the fan blades.[59] Apparently, the Raman results agreed well with the FT-IR analysis.

Cite this: DOI: 10.1039/c0xx00000x

www.rsc.org/xxxxxx

PAPER

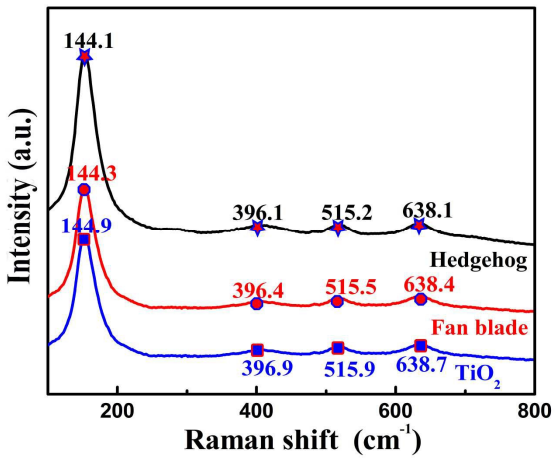

Fig. 8 Raman spectra of TiO_2 and TiO_2/ZnO hedgehogs and fan blades.

The XPS full spectra of hedgehogs and fan blades are shown in Fig. 9. The Zn 2p, O1s, Ti 2p and C 1s can be easily observed in the full spectra. The main elements are Ti, Zn, O, and C for both hedgehogs and fan blades. Among them the element of C came from the contaminants. The atomic percentages of all elements in the surfaces of hedgehogs and fan blades are given in Table 1. In TiO_2/ZnO hedgehogs, the contents of TiO_2 and ZnO are approximately 96.82% and 3.18%, respectively, as calculated from the ratio of Ti/Zn. While in TiO_2/ZnO fan blades, they are 94.89% and 5.11%. It is evident that the content of TiO_2 in the hedgehogs is higher than that in the fan blades, and TiO_2 serves as the main catalyst.

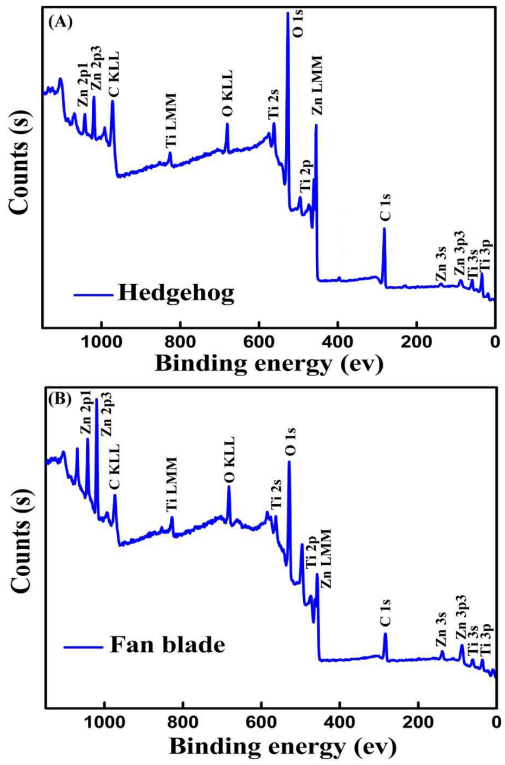

Fig. 9 XPS full spectra of hedgehogs (A) and fan blades (B).

The high resolution XPS spectra of the Ti 2p and Zn 2p regions for TiO_2 and the TiO_2/ZnO heterojunctions are given in Fig. 10. As shown in Fig. 7A, the binding energies of Ti 2p region exhibited two peaks at 458.6 and 464.7 eV, corresponding to Ti $2p_{3/2}$ and Ti $2p_{1/2}$ of Ti^{4+}, respectively. The spectra of Zn 2p depicted in Fig. 7B show two peaks at 1021.6 eV (Zn $2p_{3/2}$) and 1044.9 eV (Zn $2p_{1/2}$) of Zn^{2+}. Since there was no other Zn 2p peak appeared in the XPS spectra, Zn^{2+} ions did not enter TiO_2 lattice, but existed as a separated ZnO phase.

Table 1 The atomic percentages of elements in the surfaces of TiO_2/ZnO heterojunctions

Heterojunctions	Atomic percentage (%)			
	Ti2p	O1s	C1s	Zn2p
Fan blades	22.98	49.15	26.21	1.66
Hedgehogs	24.24	52.74	21.95	1.07

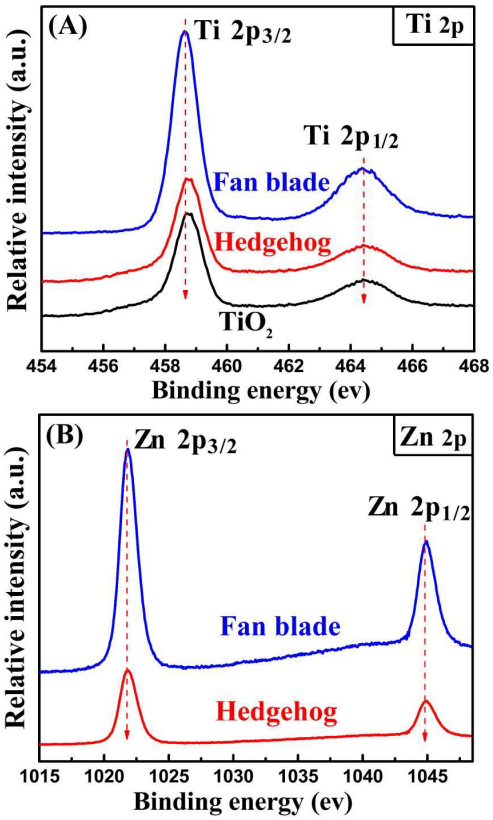

Fig. 10 High resolution XPS spectra of (A) Ti 2p region and (B) Zn 2p region for TiO_2 and TiO_2/ZnO heterojunctions.

The high resolution XPS spectra of O 1s of TiO_2 and the TiO_2/ZnO heterojunctions are shown in Fig. 11. The broad and asymmetric peak of O 1s was partitioned into two peaks, 529.8 eV and 531.2 eV (Fig. 11A), corresponding to O–Ti bonding of TiO_2 and hydroxyl group (–OH) on the surface of TiO_2/ZnO,[60] respectively. The results of curve fitting for the O 1s region of the fan blades are displayed in Fig. 11B. As shown in Fig. 11B, the full width at half maximum (FWHM) of the O 1s peak at 529.8 eV for TiO_2/ZnO was found to be slightly increased due to the overlapping of O–Zn and O–Ti bindings. This phenomenon also indicated that the coupled Zn ions existed as ZnO on the TiO_2 surface. Moreover, the surface hydroxyl groups were considered to be the chemically adsorbed H_2O, because the physically adsorbed H_2O should be easily desorbed in the super high vacuum surrounding of XPS system.[61]

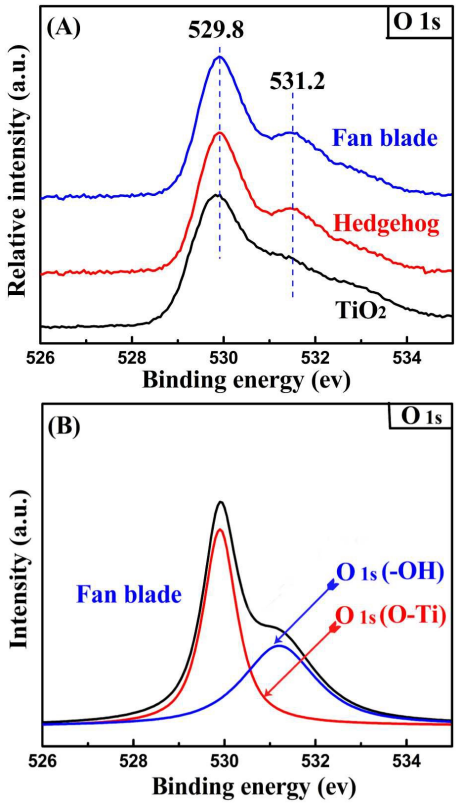

Fig. 11 High resolution XPS spectra of O 1s region for (A) TiO_2 and TiO_2/ZnO heterojunctions and (B) deconvolved peaks of TiO_2/ZnO fan blade.

The UV-vis DR spectra of the hedgehogs and fan blades are given in Fig. 12. As observed in Fig. 12, there is an obvious absorption band in the region between 200 and 400 nm, which is attributed to the electron promotion from the valence band to the conduction band.[62] In addition, the adsorption peak of ZnO at 360 nm almost disappear for both heterojunctions because of the shield effect of TiO_2 in the UV-light regime. The band gaps of the hedgehogs and fan blades in the inset, obtained by the application of the Kubelka−Munk algorithm,[63] were 2.98 and 3.04 eV, respectively, which were smaller than that of TiO_2 or ZnO. The formation of the TiO_2/ZnO heterojunctions decreased the level of the recombination of photogenerated e^-/h^+ and improved the photocatalytic ability of the ZnO/TiO_2 heterojunctions, as demonstrated by the following photocatalytic experiments.

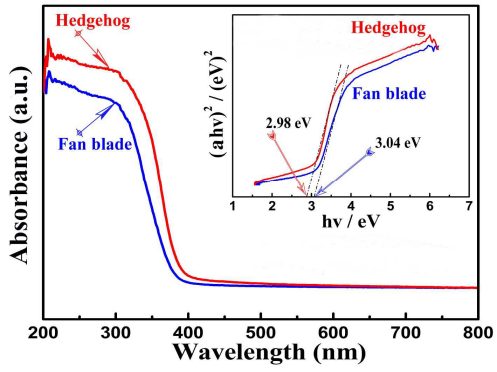

Fig. 12 UV-vis DR spectra of TiO_2/ZnO hedgehogs and fan blades. The inset shows the relationship between $(ahv)^2$ and photon energy.

Cite this: DOI: 10.1039/c0xx00000x

www.rsc.org/xxxxxx

PAPER

3.2. Photocatalytic activity of hedgehogs and fan blades

The photocatalytic performance of the TiO_2/ZnO heterojunctions were evaluated by the degradation of MO under UV-light irradiation and the results are given in Fig. 13. Figs. 13A and B show the temporal evolution of the spectral changes of MO solution. Prior to the UV-light irradiation, continuous incubation of the mixture in the dark place for 30 min led to the equilibrium adsorption of MO molecules on the surfaces of the TiO_2/ZnO heterojunctions. The major absorption peaks of MO around 462 nm diminished gradually under UV-light irradiation in the presence of the TiO_2/ZnO heterojunctions. Meanwhile, the color of suspension changed gradually, suggesting the chromophoric structure of MO was decomposed. Therefore, the UV-light photocatalytic activity of the TiO_2/ZnO heterojunctions was high. To evaluate the activity of hedgehogs and fan blades, comparative experiments of TiO_2 and ZnO particles, mechanically mixed TiO_2 and ZnO (96.82% TiO_2 and 3.18% ZnO), and commercial TiO_2 (Degussa-P25) samples were performed under the same experimental conditions as mentioned above. The relative concentration (C/C_0, C and C_0 stand for the remnant and initial concentration of MO, respectively) as a function of time is shown in Fig. 13C. After UV-light irradiation for 30 min, MO was not decomposed in the absence of photocatalyst, reflecting the high stability of MO under the UV-light. For comparison, the degradation efficiency of MO was about 97 and 85% for hedgehogs and fan blades after 30 min, respectively. It was impressive that more than 97% of MO was photodegraded by the hedgehogs after UV-light irradiation for 30 min. Meanwhile, it was noted that the TiO_2/ZnO heterojunctions exhibited remarkably superior photocatalytic activity to their counterparts of TiO_2 particles, ZnO particles, mechanically mixed TiO_2 and ZnO (96.82% TiO_2 and 3.18% ZnO), and commercial TiO_2 (Degussa-P25), from the kinetic rate constant values (Fig. 13D). Notably, the time for an entire decolorization of MO over the TiO_2/ZnO heterojunctions was about 30 min, which was much shorter than the degradation time of other TiO_2 or ZnO containing heterojunctions (listed in Table 2). It is apparent that the hedgehogs in this work have much higher photocatalytic activity; therefore, the hedgehogs are very promising for the effective removal of MO in environmental remediation.

The enhanced activity of the TiO_2/ZnO heterojunctions may arise from cumulative contributions. On one hand, the coupling of TiO_2 and ZnO in the TiO_2/ZnO heterojunctions can largely inhibit the electron−hole recombination and reduce the level of emission, resulting in more efficient charge separation and improvement in photoreaction when compared with TiO_2, ZnO or P25.[38,39] Moreover, in the absence of interfacial contact, the mechanically mixed TiO_2 and ZnO (96.82% TiO_2 and 3.18% ZnO) is unfavorable for the photocatalysis and does not achieve the desired effect. On the other hand, the uniform morphologies and high specific surface area of hedgehogs and fan blades (96 and 56 m^2 g^{-1}, respectively) may imparts multiple and long mean free path of charge carriers and maintain a large interfacial contact area to favor a heterojunction effect.

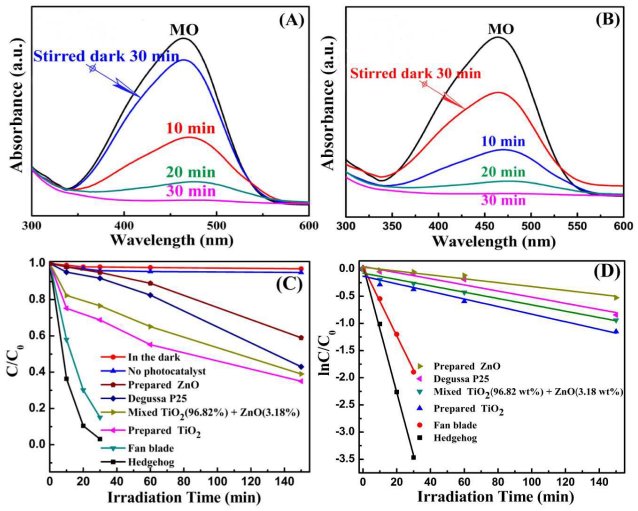

Fig. 13 Adsorption spectra of MO solutions in the presence of fan blades (A) and hedgehogs (B), (C) degradation profiles of MO over photocatalysts with different morphologies (C_0 = 20 mg L-1, catalyst = 0.1 g), (D) kinetic curves of MO degradation with photocatalysts.

The kinetic analysis of the degradation of MO is discussed in the following. The kinetic linear curves of the photocatalytic degradation of MO show that the degradation reactions follow a Langmuir-Hinshelwood apparent first-order kinetics model, described by:[67]

$$r = \frac{dC}{dt} = \frac{kKC}{1+KC} \quad (1)$$

where r is the degradation rate of the reactant (mg/(L min)), C the concentration of the reactant (mg/L), t the UV light irradiation time, k the reaction rate constant (mg/(Lmin)), and K the adsorption coefficient of reactant (L/mg). When the initial concentration (C_0) was very low (C_0=20 mg/L for MO in the present experiment), Equation (1) can be simplified to an apparent first-order model:[68]

$$\ln\frac{C_0}{C} = kKt = K_{app}t \quad (2)$$

where k_{app} is the apparent first-order rate constant (min^{-1}). The determined k_{app} values for different catalysts are summarized in Fig. 13D. The photocatalytic reactivity order is that hedgehogs > fan blades, being well consistent with the activity studies above. The higher photocatalytic efficiency of the TiO_2/ZnO hedgehogs is mainly due to the hierarchical nanostructure with high surface area.

Furthermore, repeated degradation reactions were performed

to determine the stability of the hedgehogs and fan blades. As shown in Fig. 14, the catalyst did not exhibit any significant loss of activity after five consecutive reaction cycles, indicating the outstanding stability of both photocatalysts.

Table 2 Photocatalytic activities by various TiO_2 or ZnO containing heterojunctions for MO

Photocatalyst	Degradation time (min)	Degradation rate (%)	Reference
ZnO nanorods/ TiO_2 shell	300	98.2	62
0.1% Fe-TiO_2	60	79	64
ZnO/TiO_2 composites	60	98.13	65
TiO_2/ZnO/chitosan nanocomposite	240	97	66
TiO_2/ZnO hedgehogs	30	97	This work

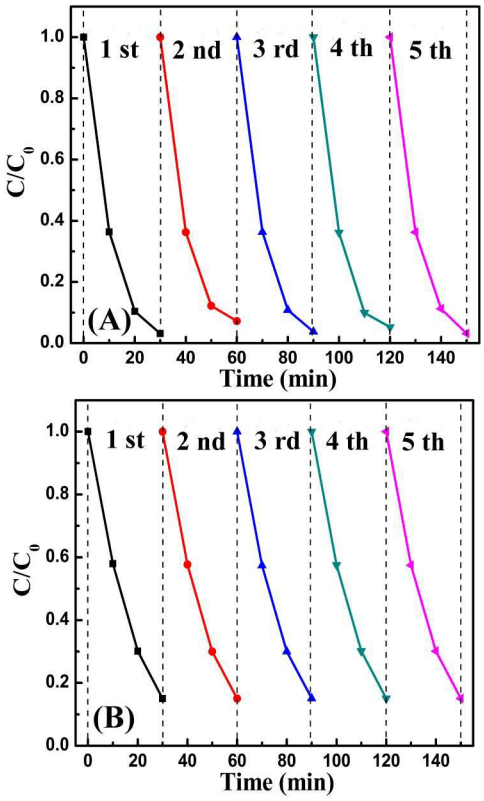

Fig. 14 Recycling tests of (A) TiO_2/ZnO hedgehogs and (B) TiO_2/ZnO fan blades for MO photodegradation under UV light irradiation.

The recombination of the photo-induced electrons and holes decreases the activity of the photocatalyst. Photoluminescence (PL) emission spectroscopy can be used to evaluate the separation capability of the photo-induced carriers, which helps understanding the efficiency of the charge carrier trapping, immigration and transfer fate in the photocatalyst.[69] The higher PL intensity usually indicates a higher recombination rate of the photo-generated electrons and holes. The PL emission spectra of TiO_2 and TiO_2/ZnO heterojunctions are shown in Fig. 15. The shape and position of the three curves seem similar. When excited by the 320 nm UV-light, two strong emission peaks at around 425 and 472 nm are observed for the three samples. The emission intensity of the TiO_2 sample is the highest, while the emission intensities of the TiO_2/ZnO heterojunctions are clearly reduced, and the hedgehogs have the lowest emission intensity. It indicates that the recombination of the photo-induced charge carriers in the TiO_2/ZnO heterojunctions is effectively inhibited. As a result, the effective charge separation in the TiO_2/ZnO heterojunctions increases the lifetime of the charge carriers and enhances the efficiency of the interfacial charge transfer, and then accounts for the high activity.

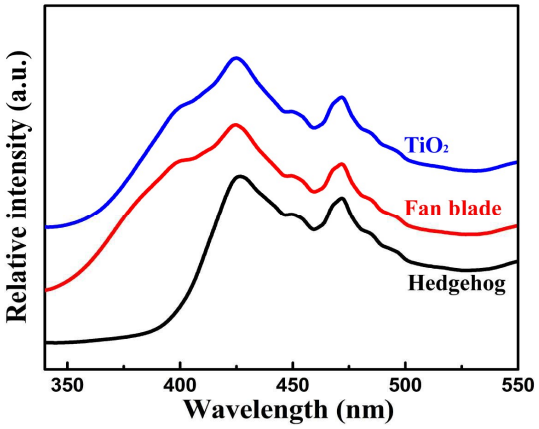

Fig. 15 Photoluminance spectra of TiO_2 and TiO_2/ZnO hedgehogs and fan blades.

The mechanism of photocatalytic decomposition over the TiO_2/ZnO heterojunctions can be delineated in Fig. 16. Although the band gap energies of ZnO and TiO_2 are similar to each other (3.37 vs. 3.2 eV), nevertheless, the potential of the conduction band (CB) and the valence band (VB) of ZnO are charged a bit more negative. When ZnO is irradiated by photon energy to surpass its band gap energy, electrons are photoexcited from the VB to the CB, leaving holes in the VB, and then electrons transfer from the CB of ZnO to the CB of TiO_2 on account of the potential difference between them, and conversely, holes transfer from the VB of TiO_2 to the VB of ZnO under UV excitation, leading to a thermal equilibrium state in this system (i.e. Fermi levels align).[70,71]

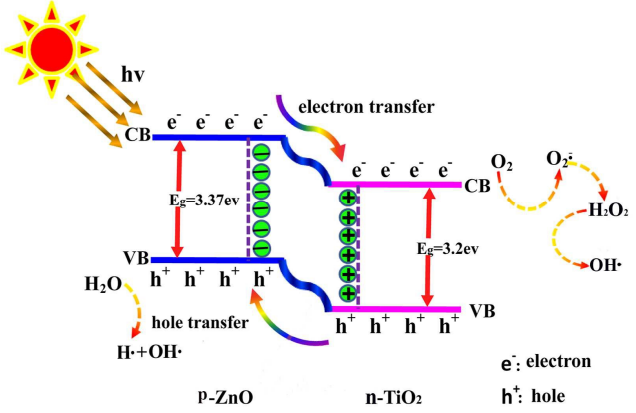

Fig. 16 Schematic diagram illustrating the formation of p-n junction and the proposed charge transfer and separation process of TiO_2/ZnO heterojunctions under UV light irradiation.

Journal of Materials Chemistry A

Cite this: DOI: 10.1039/c0xx00000x

www.rsc.org/xxxxxx

PAPER

The photocatalytic process can be proposed as follows:

$$(TiO_2\text{-}ZnO) + hv \rightarrow e^-(TiO_2) + h^+(ZnO) \quad (3)$$

$$e^- + O_2 \rightarrow O_2^{\cdot-} \quad (4)$$

$$h^+ + OH^- \rightarrow OH\cdot \quad (5)$$

$$O_2^{\cdot-} + H_2O \rightarrow HO_2\cdot + OH^- \quad (6)$$

$$HO_2\cdot + H_2O \rightarrow H_2O_2 + OH\cdot \quad (7)$$

$$H_2O_2 \rightarrow 2OH\cdot \quad (8)$$

$$OH\cdot + MO \rightarrow CO_2 + H_2O \quad (9)$$

Under UV light irradiation, the photogenerated electrons move to the TiO_2 side; meanwhile, the photogenerated holes move to the ZnO side. More importantly, due to the presence of the TiO_2/ZnO heterojunctions (i.e. potential barrier), recombination of the photogenerated electron−hole charge carriers are markedly reduced. Then the dissolved molecular oxygen reacts with electrons to yield superoxide radical anions, $O_2^{\cdot-}$. The holes are ultimately trapped by surface hydroxyl groups (or H_2O) on the surface of the photocatalyst to yield $OH\cdot$ radicals. The hydroperoxy $HO_2\cdot$ radicals and hydroxyl radicals $OH\cdot$ are immediately generated by the protonation of $O_2^{\cdot-}$. Meanwhile, highly active H_2O_2 molecules are generated by the protonation of $O_2^{\cdot-}$. Afterwards, hydroxyl radicals $OH\cdot$ are also rapidly generated by the degradation of H_2O_2 molecules. Finally, all these $OH\cdot$ serves as a strong oxidizing agent to oxidize the organic dye (MO) into CO_2 and H_2O.[72-74] Therefore, it was not surprising that the combined effects led to the enhanced photocatalytic activity.

4. Conclusions

Nanostructured TiO_2/ZnO hedgehogs and fan blades were successfully synthesized by a solvothermal method. Both TiO_2/ZnO heterojunctions exhibited enhanced photocatalytic activities in the decomposition of MO under UV-light irradiation. The degradation kinetics was pretty fast, which could be completed within 30 minutes. More importantly, the degradation capacity of the TiO_2/ZnO heterojunctions did not show any obvious decrease after five degradation cycles. The hedgehogs had the best photocatalytic activity, which could be ascribed to the hierarchical nanostructure and the higher specific surface area. This work provides a facile and economical strategy for fabricating nanostructured TiO_2/ZnO photocatalysts with tunable morphologies, and will greatly promote their industrial application to eliminate the organic pollutants from wastewater.

Notes and references

[a] *Laboratory of Solid State Ionics, School of Materials Science and Engineering, Huazhong University of Science and Technology, Wuhan 430074, P.R. China*

** Author to whom correspondence should be addressed. Tel: +86-27-87559804; Fax: +86-27-87559804; E-mail: xguo@hust.edu.cn*

1 Y. Wang, X. W. Tang, Y. M. Chen, L. T. Zhan, Z. Z. Li and Q. Tang, *J. Hazard. Mater.*, 2009, **172**, 30-37.
2 Q. Li, B. Guo, J. Yu, J. Ran, B. Zhang, H. Yan and J. R. Gong, *J. Am. Chem. Soc.*, 2011, **133**, 10878-10884.
3 M. Zhou, X. W. Lou and Y. Xie, *Nano Today*, 2013, **8**, 598-618.
4 A. Y. Zhang, L. L. Long, C. Liu, W. W. Li and H. Q. Yu, *Green Chem*, 2014, **16**, 2745-2753.
5 J. Taing, M. H. Cheng and J. C. Hemminger, *ACS Nano*, 2011, **5**, 6325-6333.
6 X. Zhang, Z. Ai, F. Jia and L. Zhang, *J. Phys. Chem. C*, 2008, **112**, 747-753.
7 J. Zhang, X. Chen, K. Takanabe, K. Maeda, K. Domen, J. D. Epping, X. Fu, M. Antonietti and X. Wang, *Angew. Chem., Int. Ed.*, 2010, **49**, 441-444.
8 R. Xie, U. Kolb, J. Li, T. Basch´e and A. Mews, *J. Am. Chem. Soc.*, 2005, **127**, 7480-7488.
9 J. S. Zhang, J. H. Sun, K. Maeda, K. Domen, P. Liu, M. Antonietti, X. Z. Fu and X. C. Wang, *Energy Environ. Sci.*, 2011, **4**, 675-678.
10 Y. Wang, W. Yang, L. Zhang, Y. Hu and X. W. Lou, *Nanoscale*, 2013, **5**, 10864-10867.
11 X. Gao, H. B. Wu, L. Zheng, Y. Zhong, Y. Hu and X. W. Lou, *Angew. Chem. Int. Ed.*, 2014, **126**, 6027-6031.
12 Y. Liu, L. Zhou, Y. Hu, C. Guo, H. Qian, F. Zhang and X. W. Lou, *J. Mater. Chem.*, 2011, **21**, 18359-18364.
13 H. Liu, J. Yuan, Z. Jiang, W. Shangguan, H. Einaga and Y. J. Teraoka, *J. Mater. Chem.*, 2011, **21**, 16535-16543.
14 A. Mukherji, R. Marschall, A. Tanksale, C. Sun, S. C. Smith, G. Q. Lu and L. Wang, *Adv. Funct. Mater.*, 2011, **21**, 126-132.
15 K. Ariga, Q. M. Ji, J. P. Hill, Y. Bando and M. Aono, *NPG Asia Mater.*, 2012, **4**, 1-11.
16 B. O'Regan and M. Gratzel, *Nature*, 1991, **353**, 737.
17 T. Nonoyama, T. Kinoshita, M. Higuchi, K. Nagata, M. Tanaka, K. Sato and K. Kato, *J. Am. Chem. Soc.*, 2012, **134**, 8841.
18 J. C. Yu, L. Z. Zhang, Z. Zheng and J. C. Zhao, *Chem. Mater.*, 2003, **15**, 2280.
19 C. Yu, G. Li, S. Kumar, K. Yang and R. Jin, *Adv. Mater.*, 2014, **26**, 892-898.
20 C. Yu, L. Wei, J. Chen, Y. Xie, W. Zhou and Q. Fan, *Ind. Eng. Chem. Res.*, 2014, **53**, 5759-5766.
21 X. Zong, H. Yan, G. Wu, G. Ma, F. Wen, L. Wang and C. Li, *J. Am. Chem. Soc.*, 2008, **130**, 7176-7177.
22 J. Jiang, X. Zhang, P. Sun and L. Zhang, *J. Phys. Chem. C*, 2011, **115**, 20555-20564.
23 C. Pan, J. Xu, Y. Wang, D. Li and Y. Zhu, *Adv. Funct. Mater.*, 2012, **22**, 1518-1524.
24 J. Zhang, Q. Xu, Z. Feng, M. Li and C. Li, *Angew. Chem., Int. Ed.*, 2008, **47**, 1766-1769.
25 K. Y. Song, M. K. Park, Y. T. Kwon, H. W. Lee, W. J. Chung and W. I. Lee, *Chem. Mater.*, 2001, **13**, 2349-2355.
26 W. L. Kostedt, A. A. Ismail and D. W. Mazyck, *Ind. Eng. Chem. Res.*,

2008, 47, 1483-1487.
27 F. Xu and L. Sun, *Energy Environ. Sci.*, 2011, **4**, 818-841.
28 X. Li, K. Lv, K. Deng, J. Tang, R. Su, J. Sun and L. Chen, *Mater. Sci. Eng. B*, 2009, **158**, 40-47.
29 A. Mclaren, T. Valdes-Solis, G. Li and S. C. Tsang, *J. Am. Chem. Soc.*, 2009, **131**, 12540-12541.
30 C. Yu, K. Yang, Y. Xie, Q. Fan, C. Y. Jimmy, Q. Shu and C. Wang, *Nanoscale*, 2013, **5**, 2142-2151.
31 Y.Liu, J. R. Jennings, S. M. Zakeeruddin, M. Grat zel and Q. Wang, *J. Am. Chem. Soc.*, 2013, **135**, 3939-3952.
32 Q. F. Zhang, T. P. Chou, B. Russo, S. A. Jenekhe and G. Z. Cao, *Angew. Chem., Int. Ed.*, 2008, **47**, 2402-2406.
33 M. García-Mota, A. Vojvodic, F. Abild-Pedersen and J. K. Nørskov, *J. Phys. Chem. C*, 2013, **117**, 460-465.
34 Q. Zhang, D. Q. Lima, I. Lee, F. Zaera, M. Chi and Y. A. Yin, *Angew. Chem.*, 2011, **123**, 7226-7230.
35 B. Subash, B. Krishnakumar, M. Swaminathan and M. Shanthi, *Langmuir*, 2013, **29**, 939-949.
36 Y. Z. Zheng, X. Tao, Q. Hou, D. T. Wang, W. L. Zhou and J. F. Chen, *Chem. Mater.*, 2011, **23**, 3-5.
37 C. Xue, T. Wang, G. Yang, B. Yang and S. Ding, *J. Mater. Chem. A*, 2014, **2**, 7674-7679.
38 W. L. Kostedt, A. A. Ismail and D. W. Mazyck, *Ind. Eng. Chem. Res.*, 2008, **47**, 1483-1487.
39 D. L. Liao, C. A. Badour and B. Q. Liao, *J. Photochem. Photobiol. A*, 2008, **194**, 11-19.
40 H. B. Jiang, L. Gao and Q. H. Zhang, *J. Inorg. Mater.*, 2003, **18**, 695-698.
41 S. G.Yang, X. Quan, X. Y. Li, Y. Z. Liu, S. Chen and G. H. Chen, *Phys. Chem. Chem. Phys.*, 2004, **6**, 659-664.
42 D. Chen, H. Zhang, S. Hu and J. H. Li, *J. Phys. Chem. C*, 2008, **112**, 117-122.
43 Q. Zhang, W. Fan and L. Gao, *Appl. Catal. B*, 2007, **76**, 168-173.
44 E. Haque, J. W. Jun and S. H. Jhung, *J. Hazard. Mater.*, 2011, **185**, 507-511.
45 M. Sevilla and A. B. Fuertes, *Energy Environ. Sci.*, 2011, **4**, 1765-1771.
46 A. Shabaev and A. L. Efros, *Nano Lett.*, 2004, **4**, 1821-1825.
47 Z. J. Gu, T. Y. Zhai, B. F. Gao, X. H. Sheng, Y. B. Wang, H. B. Fu, Y. Ma and J. N. Yao, *J. Phys. Chem. B*, 2006, **110**, 23829-23836.
48 L. S. Zhang, W. Z. Wang, Z. G. Chen, L. Zhou, H. L. Xu and W. Zhu, *J. Mater. Chem.*, 2007, **17**, 2526-2532.
49 C. L. Kuo, T. J. Kuo and M. H. Huang, *J. Phys. Chem. B*, 2005, **109**, 20115.
50 Z. R. Tian, J. A. Voigt, J. Liu, B. McKenzie, M. J. Mcdermott, M. A. Rodriguez, H. Konishi and H. F. Xu, *Nat. Mater.*, 2003, **2**, 821.
51 R. H. Zha, R. Nadimicherla and X. Guo, *J. Mater. Chem. A*, 2014, **2**, 13932-13941.
52 T. Wang, X. Yan, S. Zhao, B. Lin, C. Xue, G. Yang, S. Ding, B. Yang, C. Ma and G. Yang, *J. Mater. Chem. A*, 2014, **2**, 15611-15619.
53 Y. Huo, Y. Jin, J. Zhu and H. Li, *Appl. Catal. B: Environ*, 2009, **89**, 543-550.
54 P. M. Kumar, S. Badrinarayanan and M. Sastry, *Thin Solid Films*, 2000, **358**, 122-130.
55 F. X. Xiao, ACS Appl. Mater. Interfaces, 2012, **4**, 7055-7063.
56 F. X. Xiao, F. C. Wang, X. Z. Fu and Y. Zheng, *J. Mater. Chem.*, 2012, **22**, 2868-2877.
57 R. Georgekutty, M. K. Seery and S. C. Pillai, *J. Phys. Chem. C*, 2008, **112**, 13563-13570.
58 J. Zhang, M. J. Li, Z. C. Feng, J. Chen and C. Li, *J. Phys. Chem. B.*, 2006, **110**, 927.
59 Y. X. Wang, X. Y. Li, N. Wang, X. Quan and Y. Y. Chen, *Sep. Purif. Technol.,* 2008, **62**, 727-732.
60 J. C. Yu, J. Yu and J. Zhao, *Appl. Catal. B: Environ.*, 2002, **36**, 31-43.
61 X. Fu, L. A. Clark, Q. Yong and M. A. Anderson, *Environ. Sci. Technol.*, 1996, **30**, 647-653.
62 L. Zhu, G. Liu, X. Duan and Z. J. Zhang, *J. Mater. Res.*, 2010, **25**, 1278-1287.
63 R. S. Mane, W. J. Lee, H. M. Pathan and S. H. Han, *J. Phys. Chem. B*, 2005, **109**, 24254-24259.
64 T. Tong, J. Zhang, B. Tian, F. Chen and D. He, *J. Hazard. Mater.*, 2008, **155**, 572-579.
65 M. Ge, C. Guo, X. Zhu, L. Ma, Z. Han, W. Hu and Y, Wang, *Front. Environ. Sci. Engin. China*, 2009, **3**, 271-280.
66 H. Zhu, R. Jiang, Y. Fu, Y. Guan, J. Yao, L. Xiao and G. Zeng, *Desalination*, 2012, **286**, 41-48.
67 C. S. Turchi and D. F. Ollis, *J. Catal.*, 1990, **122**, 178-192.
68 M. S. Lee, S. S. Park, G. D. Lee, C. S. Ju and S. S. Hong, *Catal.Today*, 2005, **101**, 283–290.
69 H. Cheng, B. Huang, Y. Dai, X. Qin and X. Zhang, *Langmuir* 2010, **26**, 6618.
70 N. Serpone, P. Maruthamuthu, P. Pichat, E. Pelizzetti and H. Hidaka, *J. Photochem. Photobiol. A,* 1995, **85**, 247-255.
71 L. R. Zheng, Y. H. Zheng and C. Q. Chen, *Inorg. Chem.*, 2009, **48**, 1819-1852.
72 Z. Y. Zhang, C. L. Shao, X. H. Li, L. Zhang, H. M. Xue, C. H. Wang and Y. C. Liu, *J. Phys. Chem. C*, 2010, **114**, 7920-7925.
73 T. Aarthi and G. Madras, *Ind. Eng. Chem. Res.*, 2007, **46**, 7-14.
74 K. Rajeshwar, M. E. Osugi, W. Chanmanee, C. R. Chenthamarakshan, M. V. B. Zanoni, P. Kajitvichyanukul and R. Krishnan-Ayer, *J. Photochem. Photobiol. C*, 2008, **9**, 171-192.

Contents entry

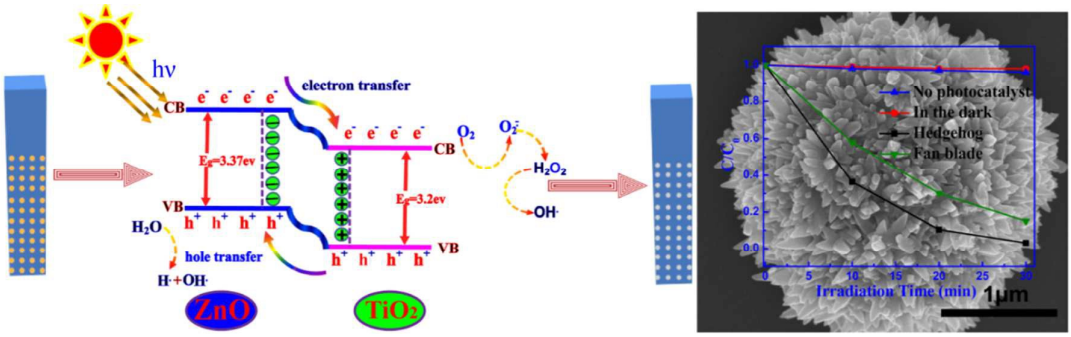

The high photocatalytic activities of TiO_2/ZnO heterojunction.